Jpn. J. Appl. Phys. Vol. 33 (1994) pp. 3197–3203
Part 1, No. 5B, May 1994

Analysis of Subsurface Imaging and Effect of Contact Elasticity in the Ultrasonic Force Microscope

Kazushi YAMANAKA[1], Hisato OGISO[1,2] and Oleg KOLOSOV[1,2,3,*]

[1]*Mechanical Engineering Laboratory, Namiki 1-2, Tsukuba, Ibaraki, 305*
[2]*Joint Research Center for Atom Technology, Higashi 1-1-4, Tsukuba, Ibaraki, 305*
[3]*Angstrom Technology Partnership, Higashi 1-1-4, Tsukuba, Ibaraki, 305*

(Received December 27, 1993; accepted for publication March 19, 1994)

We examined, both theoretically and experimentally, the characteristics of subsurface imaging with nanometer resolution and the effect of contact elasticity in the ultrasonic force microscope (UFM). In particular, the effect of the surface energy and effective elasticity on the maximum tip-sample force and the shift of the averaged tip-sample distance were examined. Furthermore, kink formation in the cantilever deflection (z_a) against the ultrasonic frequency vibration (UFV) amplitude (a) characteristics was predicted. This model was used to explain experimental observations in UFM, such as the features of the measured $z_a(a)$ curve and the damping of the cantilever torsion vibration by the UFV. Moreover, the previously reported lateral ultrasonic force microscope image of subsurface features was explained by the response of subsurface edge dislocation to a large instantaneous force enhanced by the UFV.

KEYWORDS: elasticity, surface energy, atomic force microscope, subsurface imaging, Hertzian contact, ultrasonic force microscopy

1. Introduction

As an imaging method of elastic properties and subsurface features, the scanning acoustic microscope (SAM) developed by Quate *et al.* provides the best spatial resolution comparable or superior to that of optical microscopes.[1)] Nondestructive evaluation methods of defects and elastic properties on a microscopic scale were developed using SAM, and they have been widely applied to various fields in science and technology.[2–4)] However, the spatial resolution of SAM is not always sufficient for nanometer scale defects and advanced micro/nano devices.

For materials characterization on nanometer scale, some methods using the vibration forces between the sample and a probing tip have been developed by extending the atomic force microscopy (AFM).[5)] In tunneling acoustic microscopy, the tip is vibrated[6)] and in the force modulation mode (FMM), the sample is vibrated.[7,8)] The response to the vibrating force is measured to image ion implanted layers,[6)] carbon fiber and epoxy composites[7)] and Langmuir-Blodgett films.[8)] We have developed the lateral force modulation mode (lateral FMM) to image surface gaps[9)] and friction forces[10)] on a nanometer scale.

To detect ultrasonic frequency vibration (UFV) of the scanning tunneling microscope (STM) sample, a method was developed where the nonlinear (rectifying) properties of the tunneling behavior allowed the detection of the envelope of the acoustic burst.[11)] Furthermore, Rohrbeck and Chilla detected the envelope of surface acoustic waves on an AFM sample using the nonlinear relationship between the force and the tip-sample distance.[12)] We developed a theory of the AFM response to the UFV, and suggested the possibility of evaluating the local elasticity and near-field acoustic imaging of a subsurface structure.[13)] After showing the AFM response to the UFV depending on the elastic property of objects and images in ultrasonic force microscopy (UFM) reflecting the nonlinear viscoelastic properties,[14)] we proposed a general scheme of UFM for elastic and subsurface imaging[15)] based on contact elasticity.[16)] Here, both the torsion[9,10)] as well as the deflection[7,8,12–14)] of the cantilever were monitored, and selective imaging of different types of subsurface features was achieved even in the overlapped area.[15,17)] The expected image contrast due to the contact elasticity was compared between the images obtained by UFM and the FMM, using an approximate analytic expression of the $z_a(a)$ characteristics, i.e., the additional cantilever deflection z_a as a function of the UFV amplitude a.[15)] Images of a floppy disk surface,[18,19)] deoxyribonucleic acid (DNA) molecules,[20)] mica,[21)] and polyester,[14,21)] were presented. A method for elasticity measurement, ultrasonic force spectroscopy (UFS), was attempted using the threshold behavior of the $z_a(a)$ curves, and was applied to a floppy disk surface.[18,19)]

However, in order to apply the UFM to materials evaluation, it is necessary to understand various aspects of UFM more quantitatively, by introducing a realistic model. Therefore, in this paper we present a numerical simulation model of UFM, using a semi-empirical Hertzian contact elasticity considering the surface energy.[22)] This model is used to explain experimental observation in UFM, such as the feature of the $z_a(a)$ curves and the damping of the cantilever torsion vibration by the UFV. The previously reported lateral ultrasonic force microscope image of a subsurface feature is also explained.

2. Implementation of UFM

Figure 1 illustrates our AFM/UFM. For the vertical[7,8)] and lateral[9,10)] FMM, the sample scanner is used to apply the low-frequency (0.7 to 10 kHz) vibration. For UFM at frequencies between 1 to 10 MHz, a thickness-

*On leave of absence from Institute of Chemical Physics, Russian Academy of Science, 4, Kosygin St., 117334, Moscow, Russia.

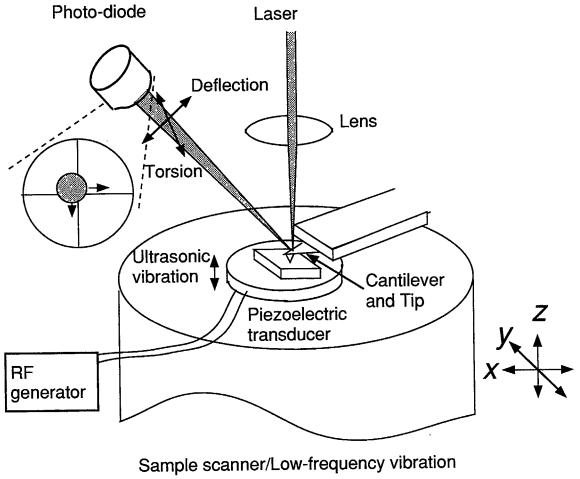

Fig. 1. Schematic illustration of UFM, installed in an atomic force microscope (AFM). A thickness-mode PZT piezoelectric transducer was bonded to a sample stage to excite ultrasonic frequency vibration (UFV) with frequencies between 1 to 10 MHz.

mode piezoelectric transducer bonded to a sample stage is used. For the lateral UFM, low-frequency lateral vibration is used together with UFV. The cantilever deflection and torsion are monitored by a four-segment photodiode. The deflection signal is used for the constant-force-mode operation of AFM,[5] and the vibrating component is measured by using a lock-in amplifier and is used for the FMM and UFM.

An advantage of sample vibration over the tip vibration scheme[6] is the flexibility in choosing the mode, frequency and direction of the vibration. The vertical or lateral vibration can be applied independently or with a certain phase relation, using a combination of piezoelectric transducers. A concave transducer was used for the UFM operation at frequencies above 100 MHz. At the bottom of the sample stage, a ZnO piezoelectric film concave transducer was sputter-deposited as shown in Fig. 2. It was employed to emit continuous waves or tone burst of focused ultrasonic waves within the sample stage. By virtue of focusing and resonance effect, the central region of the sample stage with approximate diameter of 200 μm was easily vibrated at 1-nm amplitude with electric input power of 1 mW.

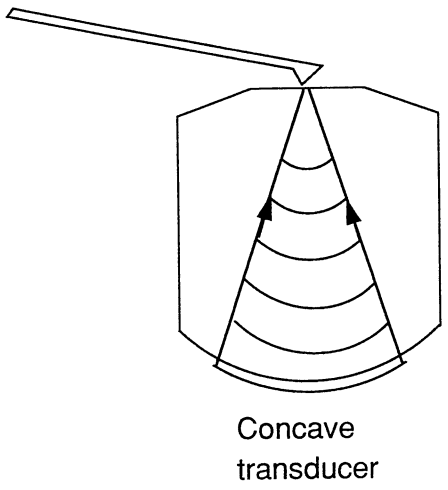

Fig. 2. A fused quartz sample stage with a ZnO piezoelectric film concave transducer deposited on its back surface. It is used to excite the high-amplitude UFV of frequencies above 100 MHz.

3. Theoretical Analysis

3.1 *Hertzian model with surface energy*

We consider the Hertzian contact model[15,16,18] in this paper, since it is the most universal elastic contact. In ambient atmosphere, attractive force due to a surface water film or adhesive forces significantly affect the tip-sample interaction. Though a number of approaches for formulating this attractive force have been presented, a simple analytical expression is not available. Recently Burnham *et al.* proposed a simplified semi-empirical formula for tip-sample force.[22] In this model the force is expressed as

$$F(d)=\frac{E^*A^3}{R}-\left(\frac{3\pi}{2}wE^*A^3\right)^{1/2}-F_{\mathrm{att}}, \tag{1}$$

or,

$$F(d)=E^*(Rd^3)^{1/2}-\left(\frac{3}{2}\pi wE^*\right)^{1/2}(Rd)^{3/4}-F_{\mathrm{att}}, \tag{2}$$

converted using the Hertzian approximation $A^2\approx Rd$. Here, the variable A is the radius of contact area, d is the tip-sample distance with the plus sign indicating increasing indentation, and R is the tip radius. The constant E^* is the effective elasticity, defined as

$$E^*=\left[\frac{(1-\nu_1^2)}{E_1}\right]+\left[\frac{(1-\nu_2^2)}{E_2}\right]^{-1}, \tag{3}$$

where E_1, ν_1 and E_2, ν_2 are Young's modulus and Poisson's ratio of the tip and sample, respectively, and w is the Dupré adhesion energy.[22] The adhesion energy w is the work per unit area of contact required to separate two solid surfaces, or the change of the surface energy per unit area of two solid surfaces due to the contact.[23]

The first term in the right-hand side of eqs. (1) and (2) gives the Hertzian repulsion, the second term gives the transition from attraction to repulsion and the third term F_{att} gives the long-range attraction force. Since we investigate the effect of the second term, we neglect F_{att} in this paper.

The force curves $F(d)$ for the effective elasticity of 50 GPa and 5 GPa, with the cantilever spring constant k of 0.2 N/m, tip radius R of 20 nm and the adhesion energy w of 360 mJ/m^2 are shown in Fig. 3. It shows nonlinear behavior, but it is necessary to note that it is due to the geometric effect of the sphere-flat contact and the adhesion energy rather than due to the intrinsic inelasticity, or nonlinear stress-strain relation. Although there is a discontinuous change of slope at $d=0$, it has no essential effect on the following analysis. This discontinuous change can be reduced or eliminated by assuming appropriate attraction term F_{att} as a function of d.[22] Although eq. (2) is quite simple, it reproduces essential features of a more elaborate theoretical treatment describing the transition from attraction to repulsion.[24]

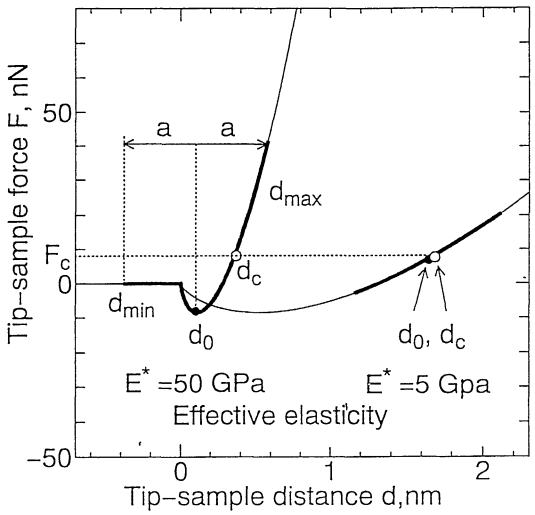

Fig. 3. Tip-sample force $F(d)$ as a function of tip-sample distance. The effective elasticity of 50 GPa and 5 GPa, with the cantilever spring constant k of 0.2 N/m, tip radius R of 20 nm and the adhesion energy w of 360 mJ/m^2 are assumed. Thick curves indicate the variation of force and distance during UFV.

3.2 *Cantilever defleclion*

Using Fig. 3, we describe the operation of UFM. First, the cantilever is deflected by z_c from its free position by applying a tip-sample static force F_c. This is a standard operation of the constant-force mode in AFM. Due to this force, the tip is indented into the sample and the magnitude of the initial indentation is determined from the force curves, $d_c=F^{-1}(F_c)$, and shown by the open circles, in Fig. 3.

When UFV is applied, the cantilever cannot follow the sample vibration due to the inertia effect, since the frequency of UFV above 1 MHz is much higher than the cantilever resonant frequency. However, due to the additional repulsive force caused by contact with the vibrated sample, the cantilever deflection is increased from z_c to z_0, determined by solving an integral equation[13]

$$kz_0=\frac{1}{T}\int_0^T F(z_s+a\cos\omega t-z_0)\,dt, \tag{4}$$

where T and ω are the period and the angular frequency of UFV, respectively, k is the cantilever spring constant and z_s is the sample stage displacement required to set z_c, determined by

$$z_s=z_c+F^{-1}(kz_c). \tag{5}$$

Once z_c is assumed, z_0 is obtained by solving eq. (4), and the additional cantilever deflection $z_a=z_0-z_c$ due to UFV is calculated as a function of a.

The $z_a(a)$ characteristics for $E^*=5$ GPa with four different static repulsive forces F_c of 4, 8, 16 and 32 nN are plotted in Fig. 4. In this figure, (a) shows the case with no adhesion energy and (b) shows the case with adhesion energy w of 360 mJ/m^2. The cantilever spring constant k and the tip radius R were assumed to be 0.2 N/m and 20 nm, respectively. These parameters were chosen to be close to those used in the experiments in

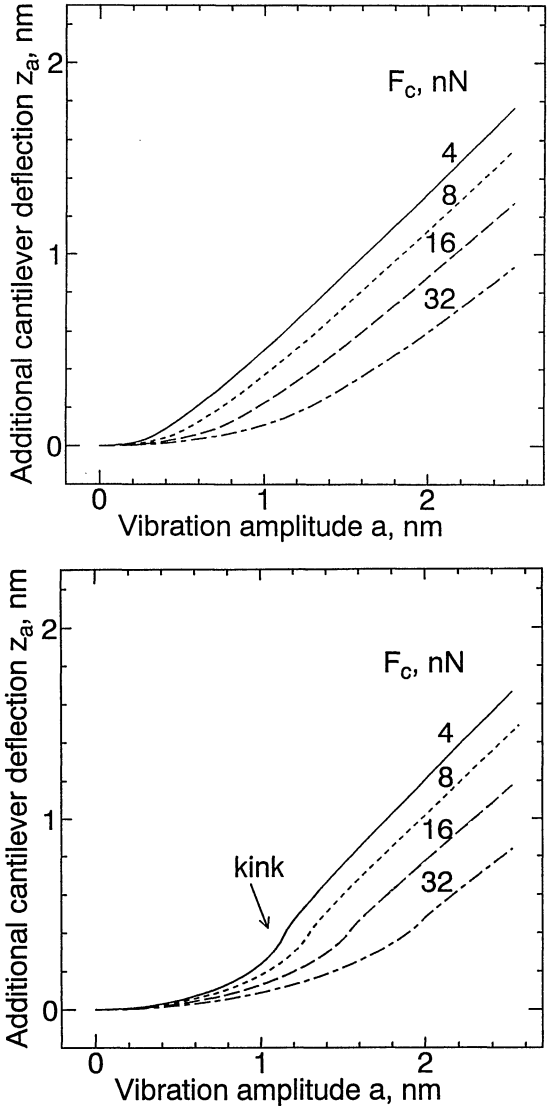

Fig. 4. Calculated additional cantilever deflection as a function of the UFV amplitude, $z_a(a)$ characteristics, for different static repulsive forces. The effective elasticity of 5 GPa, the cantilever spring constant k of 0.2 N/m, and the tip radius R of 20 nm are assumed. (a) Without adhesion energy. (b) With adhesion energy w: 360 mJ/m^2.

the order of magnitude, although not exactly adjusted to be identical.

In Fig. 4, it is seen that the deflection z_a increases with the increase of the UFV amplitude a. Although the slope $\partial z_a/\partial a$ is small at smaller a and increases at larger a, it is not easy to define a clear threshold. The deflection z_a also increases as the static repulsive force F_c decreases.[15,18] Furthermore, it is noted that the adhesion energy reduces the cantilever deflection z_a especially at small UFV amplitudes a as seen in Fig. 4(b), although at large amplitude this effect becomes less significant. Consequently, a kink is formed around a certain range of UFV amplitudes a. The kink formation is particularly obvious for smaller repulsive forces F_c of 4 and 8 nN.

The $z_a(a)$ characteristics for $F_c=8$ nN with four different effective elastic constant E^* of 1, 5, 20 and

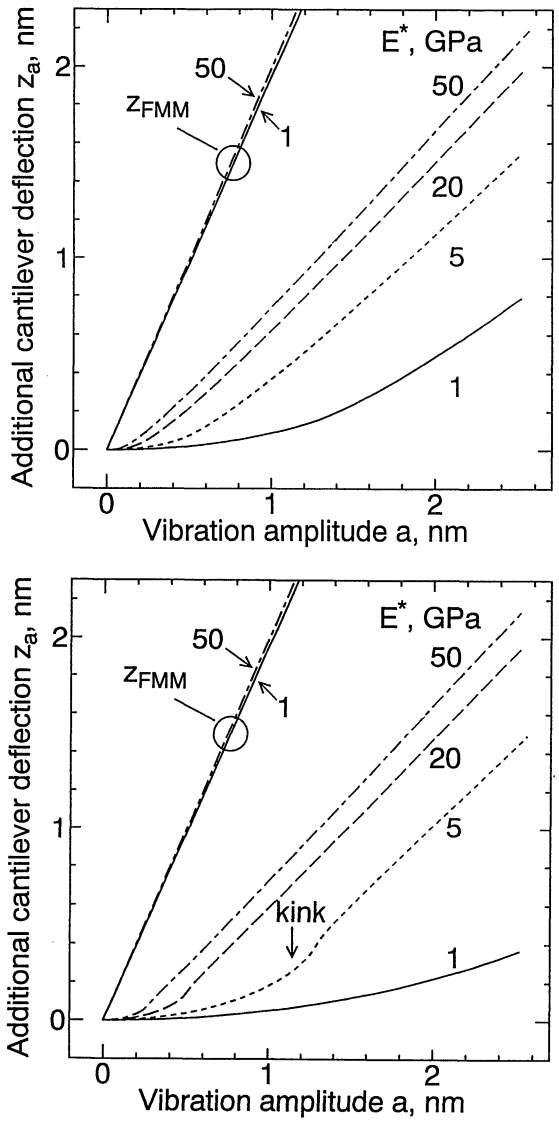

Fig. 5. Calculated additional cantilever deflection as a function of the UFV amplitude, $z_a(a)$ characteristics, for different effective elasticity. The static force of 8 nN, the cantilever spring constant k of 0.2 N/m, and the tip radius R of 20 nm are assumed. (a) Without adhesion energy. (b) With adhesion energy w: 360 mJ/m^2.

50 GPa are plotted in Fig. 5. In this figure, (a) shows the case with no adhesion energy and (b) shows that with adhesion energy w of 360 mJ/m^2. The deflection is larger for larger effective elasticity E^*. The kink formation is also observed, and the kink position is shifted to smaller UFV amplitude, as the effective elasticity E^* increases.

When the vibration frequency is much lower than the cantilever resonant frequency, we can assume that the cantilever remains in equilibrium position for each sample stage displacement z_s.[13] Then the peak-to-peak vibration amplitude of cantilever deflection z_{FMM} when the sample stage displacement is varied from z_s-a to z_s+a is given by

$$z_{FMM}=[F(d_2)-F(d_1)]/k \tag{6}$$

where d_1 and d_2 are solutions of the equations

$$F(d_1)=k(z_s-a-d_1), \quad F(d_2)=k(z_s-a-d_2). \tag{7}$$

The amplitude z_{FMM} is also plotted in Fig. 5 for two effective elasticity of $E^*=1$ GPa and 50 GPa. Since the difference between two curves is negligibly small, it will be difficult to obtain a high image contrast in the FMM images, for the elasticity difference of 1 and 50 GPa. Although the modulus of carbon and industrial graphite ranges from 3.5 GPa to 28 GPa,[22] it would be difficult to distinguish them in the FMM. This is in contrast to the UFM, where the difference for each E^* is large enough to show a significant contrast. Qualitatively, this trend agrees with the linearized spring model.[15,18] Experimentally observed high contrast in UFM and low-contrast in FMM of HOPG[15] and a floppy disk surface[18,19] are consistent with this prediction.

3.3 *Tip-sample force and distance*

During UFV, the tip-sample force F and the distance d (indentation depth) vary with time at the same ultrasonic frequency. The force and distance are important parameters for the physical process that takes place at the contact. The range of tip-sample distance d between the maximum d_{max} and minimum d_{min} for the case of the UFV amplitude a of 0.5 nm is shown as thick curves in Fig. 3. This UFV amplitude is above the kink for 50 GPa and below the kink for 5 GPa, as seen from Fig. 5(b).

The average tip-sample distance during the UFV, $d_0=z_s-z_0$, is also calculated from the solution of eq. (2). They are also indicated in Fig. 3. It should be noted that d_0 is much smaller than the initial indentation depth d_c for E^* of 50 GPa. In this force curve, the UFV amplitude is large enough to reach the nonlinear region. Then, substantial repulsive force is generated by averaging over one cycle.[13,15,18] As a result, d is shifted from the initial d_c to more separated position d_0.[25] For a given UFV amplitude, this tendency is less dominant in the-low elasticity of $E^*=5$ GPa, as shown in Fig. 3 and Table I.

The maximum instantaneous tip-sample force $F_{max}=F(z_s+a-z_0)$ is also a useful quantity to consider the deformation. As listed in Table I, the maximum force tends to increase with the effective elasticity E^*. Such tendency of the indentation and force has important implications in the interpretation of UFM images.

Table I. A numerical example of tip-sample forces and distance during the UFV of AFM samples. The constant E^* is the effective elasticity, F_{max} is the maximum tip-sample force, and d_{min}, d_{max} and d_0 are the minimum, maximum and averaged tip-sample distances during UFV. The variable d_c is the tip-sample distance under the static repulsive force without UFV. The UFV amplitude a of 0.5 nm, the tip radius of 20 nm, and the adhesion energy of 360 mJ/m^2 are assumed. Note that the difference between d_c and d_0 increased as the effective elasticity increased.

E^*, GPa	F_{max}, nN	d_{min}, nm	d_0, nm	d_{max}, nm	d_c, nm
1	12.2	4.42	4.90	5.38	4.91
5	20.7	1.16	1.64	2.12	1.68
20	36.6	0.06	0.54	1.02	0.67
50	40.5	−0.38	0.10	0.58	0.36

4. Experimental Results and Discussions

4.1 *Dependence of cantilever deflection on the UFV amplitude*

We confirmed theoretically predicted features of the $z_a(a)$ characteristics by measurement. We used a 400-nm-thick 100-μm-long Si_3N_4 cantilever mounting a Si_3N_4 tip, with the spring constant of 0.09 N/m and resonant frequency F_0 of 40 kHz. The UFV frequency was 114 MHz. Although the rigid tip-sample spring may enhance the highest possible vibration frequency of the cantilever-tip-sample system, all the linear vibration modes should be frozen at 114 MHz since this frequency is more than three orders of magnitude higher than the cantilever resonant frequency.

When the UFV at 114 MHz was amplitude-modulated at 1.0 kHz (Fig. 6, upper trace), the cantilever was vibrated at the modulation frequency as shown in lower traces of Fig. 6, where the downward direction corresponds to the increase of the cantilever deflection. The deflection z_a remained at almost zero for small amplitudes of a, and increased as the amplitude a increased over a threshold indicated by the arrow, which is consistent with previous experimental data[13,18] and theoretical analyses.[13,15,17,18] Moreover, by careful examination, it is observed that the slope of $z_a(a)$ first increased and then slightly decreased, and a kink or a deflection was formed. This kink had already been observed at lower frequencies of 1–10 MHz,[13,18] though not explained. The theoretically predicted $z_a(a)$ characteristics considering the adhesion energy given in §3.2 may explain the experimentally observed kink.

However, the magnitude of the kink changed in different experiments even on the same sample, and the reproducibility was not very good: This may be due to the change of the surface condition, and hence the adhesion energy. Therefore, atmosphere control is essential for better reproducibility and more detailed comparison with theory.

4.2 *Reduction of cantilever torsion vibration by the UFV*

We investigated the effect of the UFV amplitude on the cantilever torsion vibration on a fused quartz sample. The UFV amplitude was estimated as follows.[18] First, the additional cantilever deflection under the amplitude-modulated UFV was measured using the photodiode output voltage, which is calibrated using a DC displacement of the already calibrated piezoelectric sample scanner. Then, the UFV amplitude was approximated by the additional cantilever deflection, since these quantities are close for materials with large elasticity (fused quartz; Young's modulus of 73 GPa and Poisson's ratio of 0.17), according to Fig. 5.

When the sample was laterally vibrated at 1 kHz, cantilever torsion vibration was excited as previously reported.[10,15,17] The static repulsive force was 0.72 nN. When continuous UFV at 114 MHz was applied together with lateral vibration of the sample, the amplitude of cantilever torsion vibration was reduced as shown in Fig. 7. The torsion vibration became very small at the UFV amplitude above 1.8 nm. This damping of the torsion vibration was commonly observed on other samples such as Si or HOPG at UFV frequencies of 1–10 MHz, though the UFV amplitude required for such damping varied depending on experimental conditions.

This damping of the torsion vibration is rather surprising, since the torque that produces the cantilever

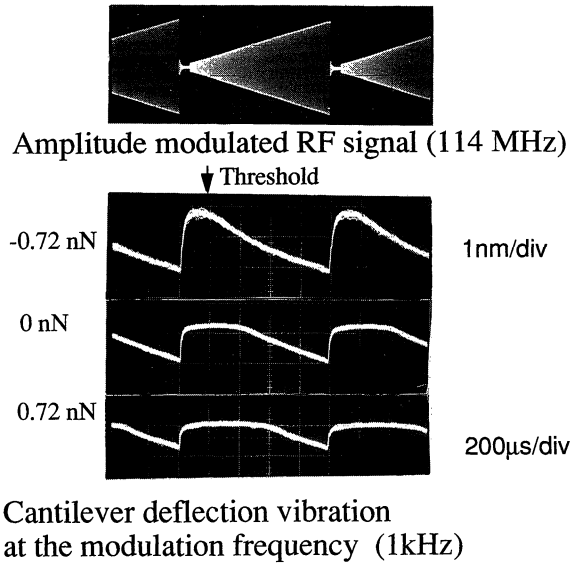

Fig. 6. Waveforms in vertical UFM. Upper trace: A sawtooth-modulated RF signal at 114 MHz for exciting the UFV on fused quartz sample stage. Lower traces: Cantilever deflection vibration signal at the modulation frequency (1 kHz) showing the measured $z_a(a)$ curves at three different static forces.

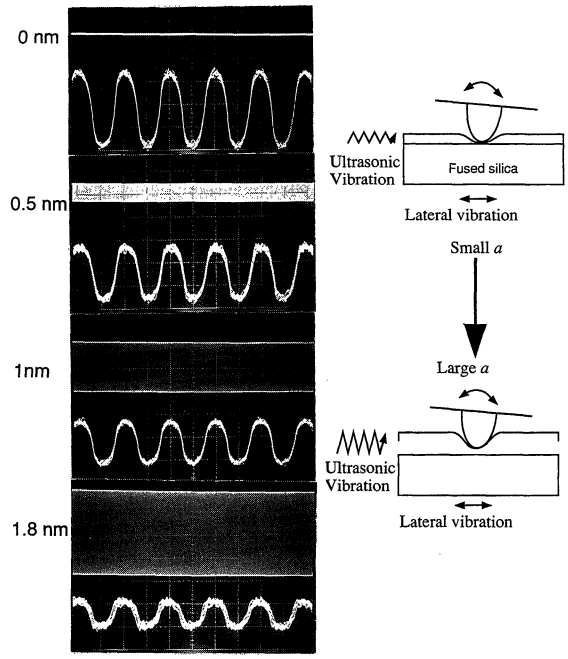

Fig. 7. Waveforms in lateral UFM. Upper traces: Continuous wave RF signal for exciting the UFV on a fused quartz sample stage at 114 MHz with the amplitude ranging between 0 and 1.8 nm. Lower traces: Cantilever torsion vibration caused by the lateral force modulation at 1 kHz. This vibration is damped by the UFV.

torsion should increase as the tip-sample force increases, and the UFV increases the maximum instantaneous tip-sample force, as well as the average force, according to the theoretical prediction given in the previous section. A possible reason for the damping of torsion vibration is that the decrease of the torque during the tip-sample detaching period of the UFV[15] is more significant than the increase of the torque during the tip-sample contact period. More detailed measurements and analysis will be the subject of a future publication.

4.3 *UFM images of subsurface features in HOPG*

We examined the effect of UFV on the lateral FMM images,[9,10] obtained from the cantilever torsion vibration signal while the sample is laterally vibrated. Figure 8(a) shows the surface plot of lateral FMM image of a highly oriented pyrolytic graphite (HOPG) sample[15] with 500×500 nm field of view. The sample was cleaved in ambient air prior to imaging. Several surface steps were clearly observed and, a few faint stringlike features were observed.

When a continuous UFV of 5.6 MHz frequency and 0.5 nm amplitude was added to the lateral vibration,

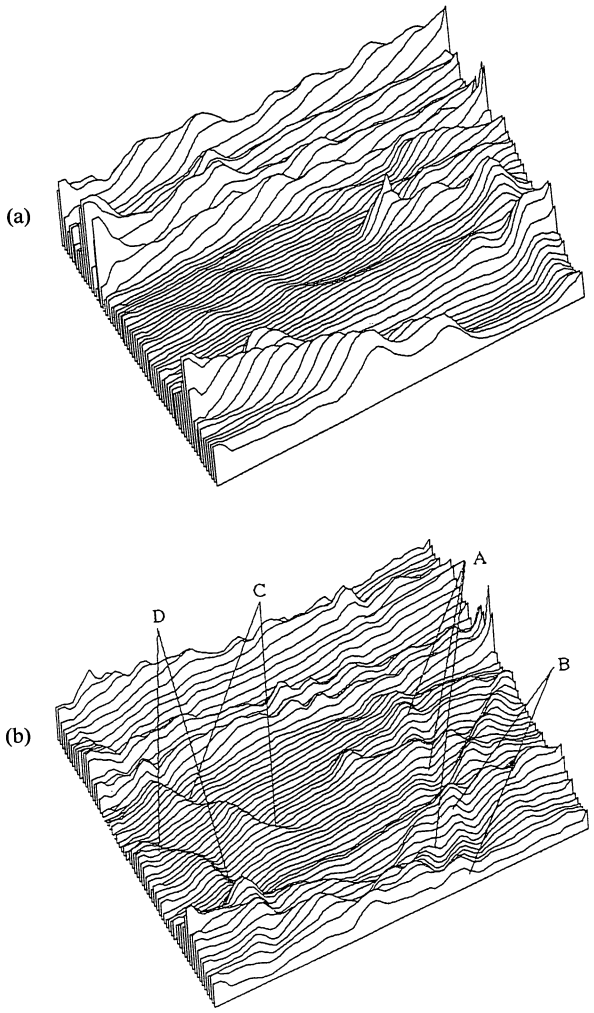

Fig. 8. Observation of subsurface features.[15] (a) Lateral FMM image of a HOPG sample with 500×500 nm field of view. (b) Lateral UFM image of the same area.

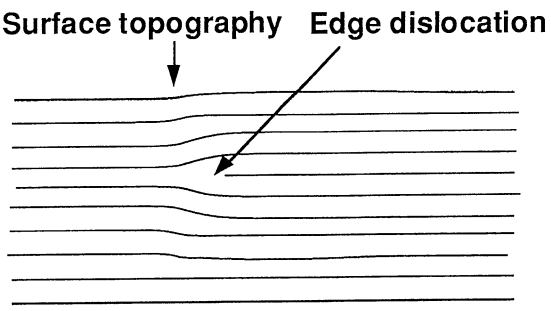

Fig. 9. Schematic illustration of a subsurface edge dislocation.

the lateral UFM image[15] was obtained as shown in Fig. 8(b). In this image, stringlike features labeled A to D were observed. Among these, A and B were not observed in the lateral FMM image, though C and D were faintly observed in the lateral FMM image. This fact indicates that A and B were perhaps located far from the surface and C and D were located close to the surface.

A possible origin of the stringlike features is edge dislocations with an extra atomic plane on one side, as illustrated in Fig. 9. Since the dislocation core has shear elasticity different from that in the perfect crystalline region, it should have a specific response to lateral UFM. If the dislocation is close to the surface, it will change the surface topography, and hence, will be observed also in topography image and lateral FMM (C and D). If the dislocation is far from the surface there will be no effect on the surface (A and B). This possibility may be examined by investigating samples with different amounts of dislocation densities, or by controlling it with annealing.

The effects of UFV on the contrast enhancement may be explained by the significantly enhanced maximum tip-sample force. Although the average tip-sample indentation depth d_0 decreases as the UFV amplitude increases, the maximum instantaneous tip-sample force is increased as shown in Fig. 3. This effect is significant when the effective elasticity is relatively large. For the case of $E^*=20$–50 GPa, the maximum tip-sample indentation force exceeds 36–40 nN (Fig. 3 and Table I). We assume that this large force causes the interaction between the tip and subsurface features, and leads to the subsurface contrast in UFM images. In contrast, if the vibration frequency is much lower than the cantilever resonant frequency, the maximum force increases only by $\Delta F \simeq ka = 0.1$ nN, when k is 0.2 N/m and a is 0.5 nm.

The large maximum tip-sample force in UFM did not damage the samples and the UFM images were reproducible, for fairly rigid solids such as HOPG. In this sense, UFM is regarded as a nondestructive imaging method of subsurface features such as the SAM[1] although the spatial resolution is significantly improved.

5. Conclusion

We examined the characteristics of subsurface imaging and the effect of the contact elasticity in UFM. In

particular, the effect of the surface energy and effective elasticity on the maximum tip-sample force and the shift of the averaged tip-sample distance were examined. Furthermore, kink formation in the cantilever deflection (z_a) against the UFV amplitude (a) characteristics was predicted. This model was used to explain experimental observation in UFM, such as the shape of the $z_a(a)$ curves, and damping of the cantilever torsion vibration by UFV. Moreover, the previously reported lateral UFM image of subsurface features was explained by the response of subsurface edge dislocations to a large instantaneous force enhanced by the UFV.

In the next step, we will investigate samples with controlled surface conditions and subsurface features. Various types of theoretical models for the surface attractive force will also be studied for more elaborate comparison with the observed $z_a(a)$ curves.

Acknowledgment

We would like to thank Professor Jun-ichi Kushibiki of Tohoku University for the deposition of the ZnO piezoelectric transducer.

1) C. F. Quate, A. Atalar and H. K. Wickramasinghe: Proc. IEEE **67** (1979) 1092.
2) J. Kushibiki: *Chouonpa Spectroscopy* (Ultrasonic Spectroscopy), eds. N. Mikoshiba and A. Ikushima (Baifu-kan, Tokyo, 1990) Vol. II, pp. 147–187 [in Japanese].
3) K. Yamanaka: *Chouonpa to Zairyou* (Materials and Ultrasonics), ed. R. Sakata, (Shokabo, Tokyo, 1992) pp. 127–146 [in Japanese].
4) A. Briggs: *Acoustic Microscopy* (Clarendon Press, Oxford, 1992).
5) G. Binnig, C. F. Quate and Ch. Gerber: Phys. Rev. Lett. **56** (1986) 930.
6) K. Takata, T. Hasegawa, S. Hosaka, S. Hosoki and T. Komoda: Appl. Phys. Lett. **55** (1989) 17.
7) P. Maivald, H. J. Butt, S. A. C. Gould, C. B. Prater, B. Drake, J. A. Gurley, V. B. Elings and P. K. Hansma: Nanotechnology **2** (1991) 103.
8) M. Radmacher, R. W. Tillmann, M. Fritz and H. E. Baub: Science **257** (1992) 1900.
9) K. Yamanaka, O. Kolosov, H. Ogiso, H. Sato and T. Koda: *Proc. Jpn. Acoust. Soc. Spring Meeting* (1993) 889.
10) K. Yamanaka, O. Kolosov, H. Ogiso, H. Sato and T. Koda: *Abstrs. for Internal Research Presentation Meet. of Mechanical Engineering Laboratory*, May 12-13, 1993, Tsukuba, Japan, p. 22.
11) A. Moreau and J. B. Ketterson: J. Appl. Phys. **72** (1992) 861.
12) W. Rohrbeck and E. Chilla: Phys. Status Solidi A **131** (1992) 69.
13) O. Kolosov and K. Yamanaka: Jpn. J. Appl. Phys. **32** (1993) L1095.
14) O. Kolosov, H. Ogiso and K. Yamanaka: *Abstrs. Internal Research Presentation Meet. Mechanical Engineering Laboratory*, May 12–13, 1993, Tsukuba, Japan, p. 19.
15) K. Yamanaka, H. Ogiso and O. Kolosov: Appl. Phys. Lett. **64** (1994) 178.
16) S. P. Timoshenko and J. N. Goodier: *Theory of Elasticity* (McGraw-Hill, London, 1970).
17) K. Yamanaka, H. Ogiso and O. Kolosov: *Proc. 14th Symp. Ultrasonic Electronics*, Dec. 7–9, 1993, Tokyo, Japan, 27.
18) O. Kolosov, H. Ogiso and K. Yamanaka: *Proc. 3rd Japan SAMPE Symp., 1993, Tokyo* (Society for Advancement of Materials and Process Engineering) p. 2196.
19) O. Kolosov, H. Ogiso and K. Yamanaka: *Abstrs. JRDC Int. Symp. Nanostructures and Quantum Effects* (Research Development Corporation of Japan, Tokyo, 1993) p. 56.
20) K. Yamanaka, O. Kolosov, and H. Ogiso: *Abstrs. JRDC Int. Symp. Nanostructures and Quantum Effects* (Research Development Corporation of Japan, Tokyo, 1993), p. 60.
21) O. Kolosov, K. Yamanaka, H. Ogiso and H. Tokumoto: *Abstrs. JRDC Int. Symp. Nanostructures and Quantum Effects* (Research Development Corporation of Japan, Tokyo, 1993) p. 58.
22) N. A. Burnham, R. J. Colton and H. M. Pollock: Nanotechnology **4** (1993) 64.
23) K. L. Johnson, K. Kendall and A. D. Roberts Proc. R. Soc. Lond. A **324** (1971) 301.
24) M. D. Pashley: Colloids & Surf. **12** (1984) 69.
25) Here, it is necessary to comment on Fig. 1 of ref. 13. First, the label z_s of the abscissa should be replaced by $z_c - z_s$, for the initial tip-sample distance to be consistent with eq. (1) of the same paper. This figure illustrates the initial tip-sample distance together with the UFV at the instant it is switched on. Therefore, the tip-sample distance is not yet shifted to the final value $z_0 - z_s$, in contrast to Fig. 3 of the present paper.